Xu *et al. Chin. J. Mech. Eng.* (2019) 32:8
https://doi.org/10.1186/s10033-019-0321-2

Chinese Journal of Mechanical Engineering

ORIGINAL ARTICLE Open Access

# Gait Analysis of Quadruped Robot Using the Equivalent Mechanism Concept Based on Metamorphosis

Kun Xu, Peijin Zi and Xilun Ding*

**Abstract**

The previous research regarding the gait planning of quadruped robot focuses on the sequence for lifting off and placing the feet, but neglects the influence of body height. However, body height affects gait performance significantly, such as in terms of the stride length and stability margin. We herein study the performance of a quadruped robot using the equivalent mechanism concept based on metamorphosis. Assuming the constraints between standing feet and the ground with hinges, the ground, standing legs and robot body are considered as a parallel mechanism, and each swing leg is regarded as a typical serial manipulator. The equivalent mechanism varies while the robot moves on the ground. One gait cycle is divided into several periods, including step forward stages and switching stages. There exists a specific equivalent mechanism corresponding to each gait period. The robot's locomotion can be regarded as the motion of these series of equivalent mechanisms. The kinematics model and simplified model of the equivalent mechanism is established. A new definition of the multilegged robot stability margin, based on friction coefficient, is presented to evaluate the robot stability. The stable workspaces of the equivalent mechanism in the step forward stage of trotting gait under different friction coefficients are analyzed. The stride length of the robots is presented by analyzing the relationship between the stable workspaces of the equivalent mechanisms of two adjacent step forward stages in one gait cycle. The simulation results show that the stride length is larger with increasing friction coefficient. We herein propose a new method based on metamorphosis, and an equivalent mechanism to analyze the stability margin and stable workspace of the multilegged robot.

**Keywords:** Quadruped robot, Gait transference, Metamorphosis, Metamorphic mechanism, Stability, Stride length

## 1 Introduction

Multilegged robots exhibit high adaptability to the environment because they do not require continuous support on the ground [1]. Therefore, they have become popular as a research topic in the recent decades. Multilegged robots include the biped robot, quadruped robot, hexapod robot, eight-legged robot, and other robots with more legs. A multilegged robot must rely on the support surface to walk. When the leg of the robot is in the stance phase, a particular constraint exists between the standing foot and support surface. While the standing leg transfers to the swing leg, the constraint is released. If we consider the constraint as a hinge, subsequently the system consists of a support surface, and the robot can be regarded as a specific mechanism. The equivalent mechanism of a multilegged robot exhibits a few similar characteristics with the metamorphic mechanism. The metamorphic mechanism is a novel mechanism proposed by DAI and JONES at the 25th ASME Biennial Mechanisms and Robotics Conference in 1998 [2]. This type of mechanism can change their topological configurations, effective links number, shapes, and degrees of freedom (DOF) [2, 3]. Unlike the traditional mechanism that only contains an unchanged topological configuration, the metamorphic mechanism has various topological configurations. Metamorphic mechanisms contain multiple configurations, and they can change their configuration to provide suitable and effective links and DOFs to adapt to different

*Correspondence: xlding@buaa.edu.cn
Robotics Institute, School of Mechanical Engineering & Automation, Beihang University, Beijing 100191, China

tasks. The metamorphic mechanism theory can be used to analyze the locomotion of multilegged robots [4, 5].

Quadruped robots not only exhibit better stability and greater load capacity than biped robots, but also has a simpler structure and easier control algorithms than hexapod robots and eight-legged robots. It can walk using statically stable gaits on complex terrains and walk quickly using dynamic stable gaits on even terrains. Research on quadruped robot focuses on structure design, kinematics analysis, dynamic analysis, gait planning, and walking control. The quadruped robot is in fact the "KUMO-I" robot [6], developed by Shigeo Hirose of the Tokyo Institute of Technology in Japan in 1976. This robot can walk by a statically stable gait. Boston Dynamics Engineering Company, in 2004, released a quadruped robot named "LittleDog" [7], that was used for machine learning, intuitive control, situational awareness, and studying topics such as irregular terrain. This company, in January 2006 and March 2008, developed two generations of quadruped robots named "BigDog" [8] for battlefield transports and, in February 2015, posted a video showing a man kicking the quadruped robot "Spot" to demonstrate the robot's capacity to regain its balance [9]. The "HyQ" robot [10–12] that was created by the Italian Institute of Technology in Italy, is combined with an electronic motor and hydraulic drive system. It can achieve jumping gait with high dynamics, high speed, and other characteristics. In 2013, MIT released the quadruped robot named "MIT cheetah", which can run at 22 km/h (6 m/s) with high efficiency [13–18]. The Tokyo Institute of Technology developed a sprawling-type quadruped robot named TITAN-XIII in 2013 that is capable of high-speed and energy-efficient walking, and a wire-driven mechanism was used to move its joint [19–21]. In 2012, the Swiss Federal Institute of Technology Zurich (ETHZ) devised the StarlETH quadruped robot [21, 22] that can trot quickly using compliant joints. Additionally, in 2016, ETHZ published a quadruped robot named ANYmal to inspect oil and gas sites. It exhibits precise torque control, and is highly robust against impulsive loads during running or jumping with various sensors [23–26]. The quadruped robot "Scalf" with a hydraulic drive system was built in Shandong university in 2012 [27–30]. This robot can run with trotting gait using the established kinematics, inverse kinematics model, and gait planning algorithms. "The Baby Elephant" designed by Shanghai Jiao Tong University used a hybrid leg mechanism [31–37]. Chen et al. [38] researched the theory to minimize the energy expenditure by optimizing the frequency and length of the stride, and were implemented in "The Baby Elephant".

A walking quadruped robot is a varying hybrid serial-parallel system [39]. In different periods, specific equivalent mechanisms are required. In the motion analysis of the quadruped robot, it is not suitable to regard the system composed of the robot and ground as a single specific mechanism [4, 40]. The locomotion of the quadruped robot can be considered as a series of moving hybrid serial-parallel mechanisms. One gait cycle of its gaits can be divided into several stages. In one stage, the system exhibits a specific mechanism. To investigate the gait performance of the quadruped robot, all the equivalent mechanisms in different stages must be studied. In the past, gait planning focused on the sequence for lifting off and placing the feet, but neglected the influence of body height. In fact, body height affects gait performance significantly, such as the stride length and stability margin.

In the context of the metamorphic theory, a new method is proposed to analyze the movement performance of multilegged robots herein. Assuming the constraints between standing feet and ground with hinges, one gait cycle is divided into several stages. In a particular stage, the ground, stance legs, and robot body form a parallel mechanism, and each swinging leg is regarded as a series manipulator. The whole system exhibits a hybrid serial-parallel mechanism. The walking movements of the multilegged robot are the motion and transition processes of these equivalent mechanisms. A new concept of stable margin is proposed to estimate the stability of gaits. A stable workspace of the equivalent mechanism in the step forward stage is analyzed. A new method to calculate the stride length of multilegged robots is presented by analyzing the relationship between the stable workspace of two adjacent mechanisms of the step forward stage in one gait cycle. The influence of friction coefficient on the stride size is analyzed, and a comparison of the stride length in different friction coefficients between the stance feet and ground are presented. The results of this study can be used to direct the motion planning of quadruped robots.

## 2 Structure and Gaits of Quadruped Robot

### 2.1 Structure of Quadruped Robot

The legs of the quadruped robot often contain three or four links. A leg with three links contains three rotation joints, whereas that with four links contains four rotation joints. We herein discuss the quadruped robot whose legs contain three links, named hip link, thigh link, and calf link from the top to bottom, as shown in Figure 1. The thigh link is connected to the hip link and calf link through the hip joint and knee joint, respectively, whose axes are parallel. Meanwhile, the hip link is connected to the body by the waist joint whose axis is parallel to the longitudinal axis of body, and perpendicular to the axes of the hip and knee joint. Slip is absent when the robot

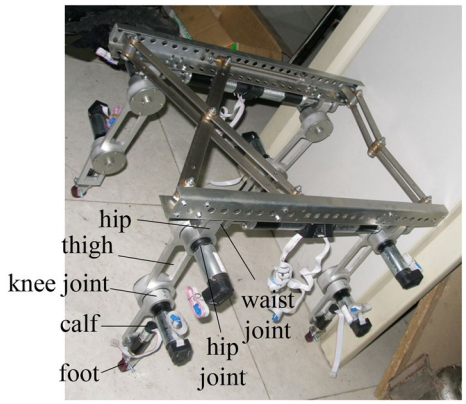


**Figure 1** Configuration of the exoskeleton arm system

walks stably on the ground. When the robot is in a stable state, the constraints between the stance feet and ground can be equivalent to those of the virtual spherical pair. According to this equivalence principle, the equivalent mechanism of the quadruped robot is as shown in Figure 2, where all legs are in the stance phase.

### 2.2 Typical Gaits of Quadruped Robot

A quadruped robot can walk with statically and dynamically stable gaits. In the statically stable gait, each leg of the robot is lifted up and down sequentially, and there are three stance legs at the least at any moment. This type of gait is named creeping gaits [41]. One gait cycle can be divided into eight different periods of movement. At the beginning of walking, the initial equivalent as shown in Figure 2, where four legs are in the stance phase. When one of the legs are lifted, it is transferred to the swing phase; we call this period the step forward stage. In this stage, the equivalent mechanism is as shown in Figure 3. From this, the leg falls and is in contact with the ground until the next leg lifts off; this period is called the switching stage. The equivalent

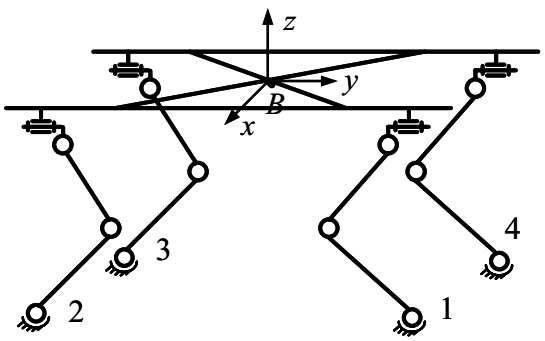


**Figure 2** Equivalent mechanism of robot with four standing legs

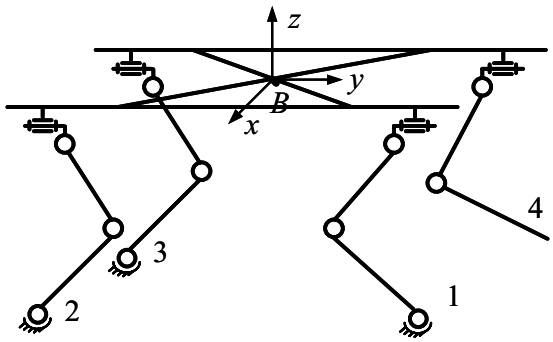


**Figure 3** Equivalent mechanism of robot with three stance legs

mechanism at this moment exhibits the same configuration as that of the initial period; however, the legs contain different position parameters with the initial period. Four legs of the quadruped robot repeat the motion individually in a certain order from the stance phase to the swing phase, to achieve walking using creeping gait. The step forward stage and switching stage occur alternately while the robot walks. The locomotion of the quadruped robot can be regarded as the movement of these series equivalent mechanisms. Figure 4 shows the sequence of equivalent mechanisms in one gait cycle. The efficiency of this gait is low because its minimum duty factor is 3/4.

Dynamic stable gaits are often used in quadruped robots to walk and run owing to their efficiency, such as trotting gait, pace gait, bounce gait, and gallop gait [42]. We used the trotting gait in our study. One gait cycle of this gait can be divided into four different periods of movement. In the beginning of the trotting gait, the equivalent mechanism is as shown in Figure 2. When two of the legs are in the same diagonal lift, transferring to the swing phase, the equivalent mechanism of this step forward stage is as shown in Figure 5. After this stage, the locomotion enters the switching stage, and the two legs are in contact with the ground until the other two legs lift off. The equivalent mechanisms of the switching stages exhibit the same configuration as that of the initial period. The four legs of the quadruped robot repeat the motion two by two in a certain order, from the stance phase to the swing phase to achieve walking using the trotting gait. The step forward stage and switching stage occur alternately while the robot walks. The locomotion of the quadruped robot can be regarded as the movement of these series equivalent mechanisms. Figure 6 shows the sequence of the equivalent mechanisms in one gait cycle. The efficiency of this gait is higher than that of the statically stable gait because its minimum duty factor is 1/2.

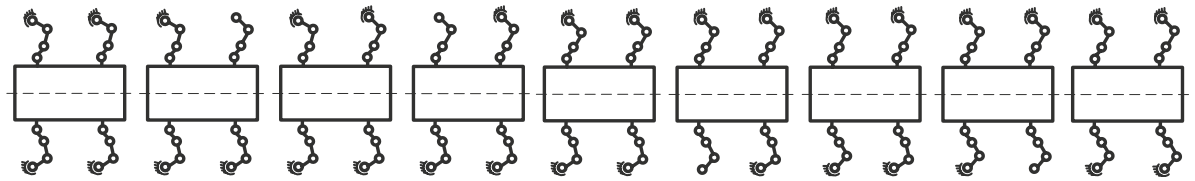

**Figure 4** Sequence of equivalent mechanisms in one cycle of creeping gait

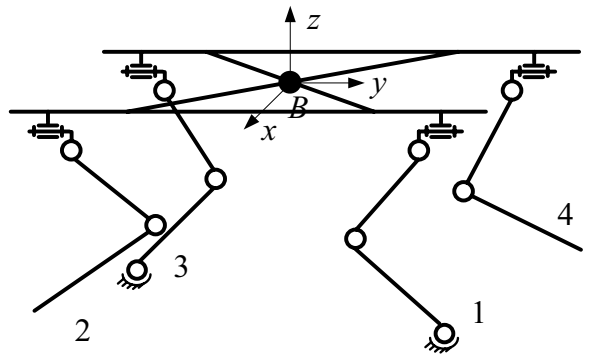


**Figure 5** Equivalent mechanism of robot in step forward stage of trotting gait

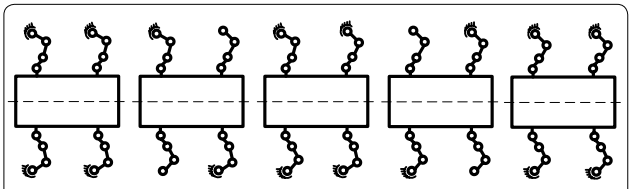

**Figure 6** Sequence of equivalent mechanisms in one cycle of trotting gait

Other gaits exhibit similar characteristics with these two gaits; their walking can be regarded as a movement of a series of equivalent mechanisms. We do not discuss them herein.

### 2.3 Gait Transference

A quadruped robot can change its gait while it walks on the ground. In this study, we refer to the creeping gait and trotting gait to introduce the transformation process between different gaits of the quadruped robot. When a quadruped robot walks using the creeping gait, a switching stage must occur at a certain moment. At this moment, the equivalent mechanism of the quadruped robot involves four standing legs. In the next time period, the robot can choose its two stance legs to transfer to the swing legs, such that the creeping gait of the robot can be changed to trotting gait. Similarly, the trotting gait can be changed to creeping gait while the quadruped robot walks on the ground. These two transformation processes are shown in Figure 7. Analogously, other gaits can be changed with each other.

## 3 Kinematics of Quadruped Robot

This section describes the kinematics of the quadruped robot. Because of the different equivalent mechanisms of the robot in different periods, we must establish the general kinematics for the quadruped robot. For each equivalent mechanism, there exists the stance legs, swing legs, or these two types combined. Therefore, we establish the kinematics for the swing leg and stance leg, separately. The forward kinematics equations are established through the product of the exponential formula, and the inverse kinematics are derived by the geometric method.

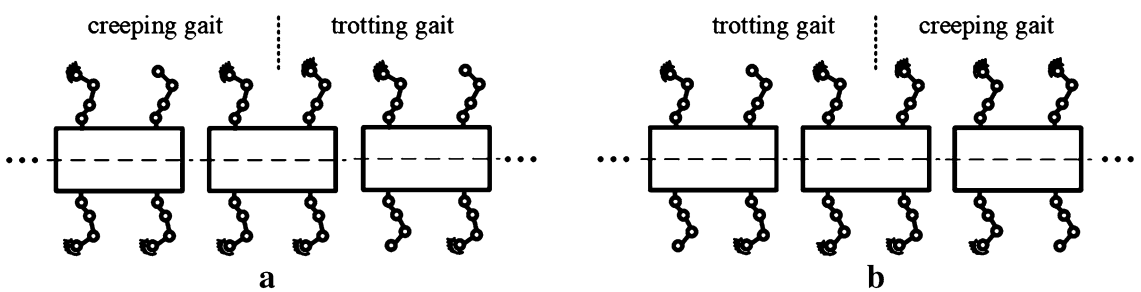


**Figure 7** Transformation processes between creeping gait and trotting gait

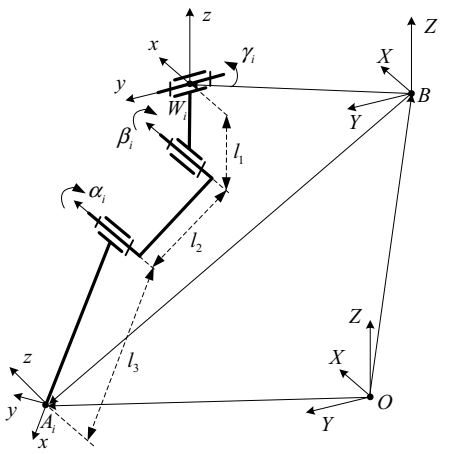


**Figure 8** Mechanism of swing leg *i*

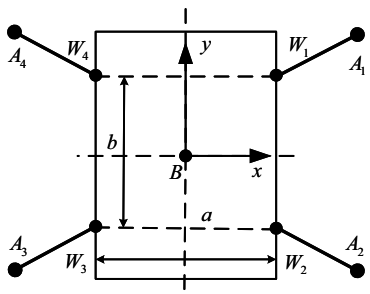


**Figure 9** Projection diagram of the robot in chassis plane

### 3.1 Forward Kinematics of Swing Leg

Figure 8 shows the mechanism of the swing leg. Four frames have been established for the kinematics analysis: the global reference frame $\{O\}$, and the body reference frame $\{B\}$ that is fixed on the geometrical center of the robot body and moves with the body (Figure 9); the single leg reference frame $\{W_i\}$, which is established at the waist joint and fixed to the chassis of the robot, and the foot reference frame $\{A_i\}$ which is located at the end of the swinging leg $i$ (foot of swinging leg $i$). The configuration when all legs are fully extended is chosen as the home configuration. In this position, all the joint variables are assumed to be zero.

Because frame $\{B\}$ and frame $\{W_i\}$ are both fixed on the robot body, the transformation matrix from frame $\{B\}$ to frame $\{W_i\}$ is constant and can be given as follows:

$$g_{BW_i} = \begin{pmatrix} I & {}^b p_{W_i} \\ 0 & 1 \end{pmatrix},$$

where ${}^b p_{W_i}$ is a $3 \times 1$ position vector,

$${}^b\boldsymbol{p}_{W_1} = \begin{pmatrix} a/2 \\ b/2 \\ -c \end{pmatrix}, {}^b\boldsymbol{p}_{W_2} = \begin{pmatrix} -a/2 \\ b/2 \\ -c \end{pmatrix},$$
$${}^b\boldsymbol{p}_{W_3} = \begin{pmatrix} -a/2 \\ -b/2 \\ -c \end{pmatrix}, {}^b\boldsymbol{p}_{W_4} = \begin{pmatrix} a/2 \\ -b/2 \\ -c \end{pmatrix}.$$

The transformation matrix from frame $\{W_i\}$ to frame $\{A_i\}$ at the home configuration can be given as follows:

$$g_{W_iA_i}(\boldsymbol{0}) = \begin{pmatrix} & & 0 \\ \boldsymbol{R}_{W_iA_i} & & -(l_1+l_2+l_3) \\ & & 0 \\ \boldsymbol{0} & & 1 \end{pmatrix},$$

where $\boldsymbol{R}_{W_iA_i} = \begin{pmatrix} -1 & 0 & 0 \\ 0 & 1 & 0 \\ 0 & 0 & -1 \end{pmatrix}$.

Twist $\xi_{ij}$ for each joint is introduced to describe the screw motion of the $j$th joint of the $i$th leg. The twist for a rotation joint can be represented by

$$\boldsymbol{\xi}_{ij} = \begin{pmatrix} \boldsymbol{\omega}_{ij} \\ \boldsymbol{r}_{ij} \times \boldsymbol{\omega}_{ij} \end{pmatrix}, \tag{1}$$

where $\boldsymbol{\omega}_{ij} = \left({}^x\omega_{ij}, {}^y\omega_{ij}, {}^z\omega_{ij}\right)^{\mathrm{T}}$ is the direction of the screw axis; $\boldsymbol{r}_{ij} = \left({}^x r_{ij}, {}^y r_{ij}, {}^z r_{ij}\right)^{\mathrm{T}}$ is the vector of any point on the axis.

Subsequently, the forward kinematics of the swing leg $i$ is given by the product of the exponentials:

$$\boldsymbol{g}_{OA_i}(\boldsymbol{\theta}) = \boldsymbol{g}_{OB}\boldsymbol{g}_{BW_i} e^{\gamma_i \hat{\xi}_{i1}} e^{\beta_i \hat{\xi}_{i2}} e^{\alpha_i \hat{\xi}_{i3}} \boldsymbol{g}_{W_iA_i}(\boldsymbol{0}), \tag{2}$$

where $\gamma_i$ is the waist joint variable, $\beta_i$ is the hip joint variable, $\alpha_i$ is the knee joint variable, and $g_{OB}$ is the transformation matrix from frame $\{O\}$ to frame $\{B\}$,

$$g_{OB}\begin{pmatrix} {}^o\boldsymbol{R}_B & {}^o\boldsymbol{p}_B \\ \boldsymbol{0} & 1 \end{pmatrix}$$

with ${}^o\boldsymbol{R}_B$ a $3 \times 3$ rotation matrix, indicating the orientation of the robot body relative frame $\{O\}$, and ${}^o\boldsymbol{p}_B$ is a $3 \times 1$ position vector, ${}^o\boldsymbol{p}_B = \left({}^o x_b, {}^o y_b, {}^o z_b\right)^{\mathrm{T}}$, that denotes the position of point B relative to frame $\{O\}$.

### 3.2 Forward Kinematics of Standing Leg

This section describes the forward kinematics of the standing leg. Three mutually perpendicular rotation joints replace the virtual spherical joint. Four frames are established, as shown in Figure 10. Frame $\{O\}$ is built as the global reference frame. The body reference frame $\{B\}$ is fixed on the robot body and moves with the body. The leg reference frame $\{W_i\}$ is established at the waist

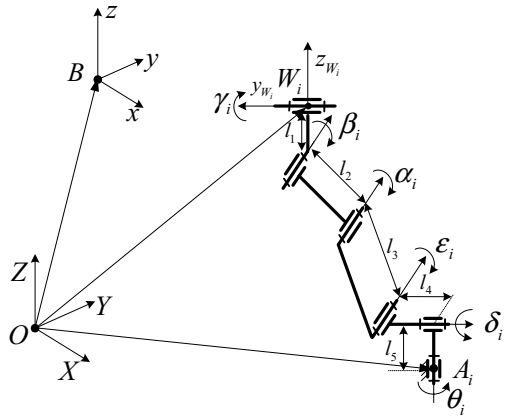


**Figure 10** Mechanism of stance leg *i*

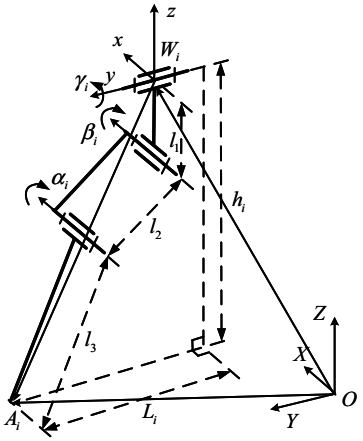


**Figure 11** Mechanism sketch of leg *i* in space

joint and fixed to the body of robot, and the foot reference frame $\{A_i\}$ is located at the foot of the supporting leg *i*. The configuration when the leg is fully extended is regarded as the home configuration. In this position, all the joint variables are set to zero.

Because $l_4$ and $l_5$ are parameters of the virtual sphere joint, they are equal to zero. The transformation matrix from frame $\{A_i\}$ to frame $\{B\}$ at the home configuration is represented by

$$\boldsymbol{g}_{A_iB}(\mathbf{0}) = \begin{pmatrix} \boldsymbol{I}_{3\times3} & {}^{A_i}\boldsymbol{p}_B \\ \mathbf{0} & 1 \end{pmatrix},$$

where ${}^{A_i}\boldsymbol{p}_B$ is a $3\times1$ position vector,

$${}^{A_1}\boldsymbol{p}_B = \begin{pmatrix} -a/2 \\ -b/2 \\ -(l_1+l_2+l_3) \end{pmatrix}, {}^{A_2}\boldsymbol{p}_B = \begin{pmatrix} a/2 \\ -b/2 \\ -(l_1+l_2+l_3) \end{pmatrix},$$

$${}^{A_3}\boldsymbol{p}_B = \begin{pmatrix} a/2 \\ b/2 \\ -(l_1+l_2+l_3) \end{pmatrix}, {}^{A_4}\boldsymbol{p}_B = \begin{pmatrix} -a/2 \\ b/2 \\ -(l_1+l_2+l_3) \end{pmatrix}.$$

According to Eq. (1), all joint twists can be obtained and the forward kinematics of the supporting leg *i* is given in the following:

$$\boldsymbol{g}_{OB}(\boldsymbol{\theta}) = \boldsymbol{g}_{OA_i} e^{\theta_i\hat{\xi}_{i1}} e^{\delta_i\hat{\xi}_{i2}} e^{\varepsilon_i\hat{\xi}_{i3}} e^{\alpha_i\hat{\xi}_{i4}} e^{\beta_i\hat{\xi}_{i5}} e^{\gamma_i\hat{\xi}_{i6}} \boldsymbol{g}_{A_iB}(\mathbf{0}), \tag{3}$$

where $\varepsilon_i$, $\delta_i$ and $\theta_i$ are the variables of the virtual sphere joint. $g_{OA_i}$ is the transformation matrix from frame $\{O\}$ to frame $\{A_i\}$,

$$g_{OA_i} = \begin{pmatrix} {}^{o}\boldsymbol{R}_{A_i} & {}^{o}\boldsymbol{p}_{A_i} \\ \mathbf{0} & 1 \end{pmatrix}$$

with ${}^{o}\boldsymbol{R}_{A_i}$ a $3\times3$ rotation matrix that indicates the orientation of the frame $\{A_i\}$ relative to frame $\{O\}$, and ${}^{o}\boldsymbol{p}_{A_i}$ is a $3\times1$ position vector, ${}^{o}\boldsymbol{p}_{A_i} = \left({}^{o}x_{A_i}, {}^{o}y_{A_i}, {}^{o}z_{A_i}\right)^{\mathrm{T}}$, that denotes the position of point $A_i$ relative to frame $\{O\}$.

### 3.3 Inverse Kinematics of Robot

We used the geometric approach to obtain the inverse kinematics solution. In the geometric approach, the spatial geometry problem can be decomposed into several plane-geometry problems. Because of the simple structure of the robot leg, this can be performed easily. The variables of each leg joint (joint angles) can be solved using the tools of the plane geometry.

For leg *i* with 3 DOFs as shown in Figure 11, the vectors ${}^{o}\boldsymbol{p}_{W_i}$ and ${}^{o}\boldsymbol{p}_{A_i}$ that are the position of points $W_i$ and $A_i$, respectively, relative to the coordinate system $\{O\}$ are known, and the orientation of frame $\{W_i\}$ relative to the frame $\{O\}$, ${}^{o}_{w_i}\boldsymbol{R}$ is given. The position of point $A_i$ relative to $\{O\}$ can be obtained:

$${}^{o}\boldsymbol{p}_{A_i} = {}^{o}\boldsymbol{p}_{W_i} + {}^{o}\boldsymbol{p}_{W_iA_i}, \tag{4}$$

where ${}^{o}\boldsymbol{p}_{W_iA_i}$ is the description of vector $W_iA_i$ relative to $\{O\}$. Using the rotation transformation, Eq. (4) can be written as follows:

$${}^{o}\boldsymbol{p}_{A_i} = {}^{o}\boldsymbol{p}_{W_i} + {}^{o}_{w_i}\boldsymbol{R}\,{}^{w_i}\boldsymbol{p}_{A_i}, \tag{5}$$

where ${}^{w_i}\boldsymbol{p}_{A_i}$ is the position of point $A_i$ relative to frame $\{W_i\}$. Therefore, we can obtain ${}^{w_i}\boldsymbol{p}_{A_i}$ as follows:

$${}^{w_i}\boldsymbol{p}_{A_i} = {}^{w_i}_{o}\boldsymbol{R}\left({}^{o}\boldsymbol{p}_{A_i} - {}^{o}\boldsymbol{p}_{W_i}\right) = {}^{o}_{w_i}\boldsymbol{R}^{-1}\left({}^{o}\boldsymbol{p}_{A_i} - {}^{o}\boldsymbol{p}_{W_i}\right). \tag{6}$$

Because the axis of the knee joint is parallel to the axis of the hip joint, and is perpendicular to the axis of waist joint, the leg is planar and the projection in the body chassis plane of the leg is a straight line. According to

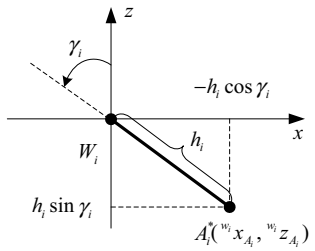


**Figure 12** Leg *i* projection onto *xz* plane of frame $\{W_i\}$

the geometrical relationship shown in Figure 11, we can obtain

$$\begin{cases} h_i = l_1 + l_2\cos\beta_i + l_3\cos(\alpha_i+\beta_i), \\ L_i = l_2\sin\beta_i + l_3\sin(\alpha_i+\beta_i), \end{cases} \tag{7}$$

where $L_i$ is the projection length of leg $i$ in the $xy$ plane of frame $\{W_i\}$, and $h_i$ is the projection length from foot $A_i$ to the $xz$ plane of frame $\{W_i\}$.

Figure 12 shows the projection of leg $i$ onto the $xz$ plane of $\{W_i\}$. Therefore, we can obtain the following equations:

$$\begin{cases} h_i = \sqrt{{}^{w_i}x_{A_i}^2 + {}^{w_i}z_{A_i}^2}, \\ L_i = {}^{w_i}y_{A_i}, \\ \tan(3\pi/2+\gamma_i) = {}^{w_i}z_{A_i}/{}^{w_i}x_{A_i}, \end{cases} \tag{8}$$

where $({}^{w_i}x_{A_i}\ {}^{w_i}y_{A_i}\ {}^{w_i}z_{A_i})$ is given to specify the position of point Ai relative to frame $\{W_i\}$.

If the position of point $A_i$ relative to frame $\{O\}$, and the position and orientation of the robot body relative to frame $\{O\}$ are known, the variables of leg $i$, $\alpha_i$, $\beta_i$, $\gamma_i$ can be solved by Eqs. (6)–(8).

## 4 Stability Analysis of Typical Gaits

In previous studies, the evaluation of statically stable gaits depends on the relationship between the vertical projection of the center of mass and the support polygon. If the vertical projection of the center of mass is located in the support polygon, the robot is stable; otherwise, the robot is not in the stable state. This approach ignores the impact of inertial force generated by the acceleration and deceleration of the robot. The "stability margin" is defined as the shortest distance from the vertical projection of the center of gravity to the boundaries of the support pattern in the horizontal plane [43]. However, in some cases, despite the vertical projection of the robot's center of mass being in the support polygon, the reaction force of the ground required owing to the acceleration of the robot exceeds the force that the ground can provide. If the standing feet slips on the ground, the robot will not be in a stable state. Quadruped robots often use the dynamic stable gait to obtain high walking efficiency. The zero-moment point (ZMP) if often used to estimate the dynamic stability of robots [44]. When the ZMP is located in the standing foot, the robot is stable; otherwise, it is not. The "stability margin" of the dynamic stable gaits are defined as the shortest distance from the ZMP to the boundaries of the support pattern [45].

In fact, multilegged robots depend on the reactive force from the supporting face to maintain balance. If the supporting face can provide adequate reactive force, the robot can be stable. In this case, the ZMP of the robot is located in the support polygon. Otherwise, the robot is unstable.

The force diagram of the stance foot $i$ is shown in Figure 13. The reactive force is composed of one force vector $\boldsymbol{F}_{A_i} = \left(f_{A_i}^x\ f_{A_i}^y\ f_{A_i}^z\right)$, and one moment vector $\boldsymbol{\tau}_{A_i} = \left(\tau_{A_i}^x\ \tau_{A_i}^y\ \tau_{A_i}^z\right)$. The constraints between the standing foot and ground must satisfy the equation as follows:

$$\sqrt{(f_{A_i}^x)^2 + (f_{A_i}^y)^2} \le \mu f_{A_i}^z, \tag{9}$$

where $\mu$ is the static friction coefficient. Here, we choose the coefficient of sliding friction instead of the static friction coefficient.

The stability margin of the multilegged robot with one stance leg can be defined as

$$S_d = 1 - \frac{\mu'}{\mu}, \tag{10}$$

where $\mu' = \frac{\sqrt{\left(f_{A_i}^x\right)^2 + \left(f_{A_i}^y\right)^2}}{f_{A_i}^z}$. While $f_{A_i}^z = 0$, $f_{A_i}^x = f_{A_i}^y = 0$; subsequently, $\mu' = 0$. While $f_{A_i}^z = 0$, $f_{A_i}^x = f_{A_i}^y \neq 0$; subsequently, $\mu' = +\infty$.

The stability margin of the multilegged robot with $n$ standing legs can be defined as

$$S_d = \min\left(S_d^1\ S_d^2\ \cdots\ S_d^n\right), \tag{11}$$

where $S_d^i = 1 - \frac{\mu_i'}{\mu}$.

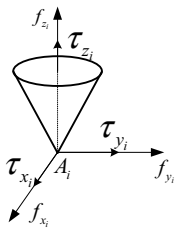


**Figure 13** Force diagram of standing foot *i*

When $S_d > 0$, the robot is in the stable state. When $S_d < 0$, the robot is in the unstable state. When $S_d = 0$, the robot is in the critical stable state.

From Eq. (10) and Eq. (11), we can find that the stability of the multilegged robot depends primarily on the friction coefficient between the standing foot and ground.

We can combine the force vector and moment vector together, to form a new vector:

$$\boldsymbol{W}_{A_i} = \left(f_{A_i}^x, f_{A_i}^y, f_{A_i}^z, \tau_{A_i}^x, \tau_{A_i}^y, \tau_{A_i}^z\right)^{\mathrm{T}}.$$

On the CoM of the robot, a similar vector exists: $\boldsymbol{W}_c = \left(f_{x_c}, f_{y_c}, f_{z_c}, \tau_{x_c}, \tau_{y_c}, \tau_{z_c}\right)^{\mathrm{T}}$. If we ignore the influence of external forces, then $\tau_{x_c} = \tau_{y_c} = \tau_{z_c} = 0$, $f_{x_c} = m_c a_c^x$, $f_{y_c} = m_c a_c^y$, and $f_{z_c} = m_c a_c^z + m_c g$.

For $n$ stance legs,

$$\sum_{i=1}^{n} \boldsymbol{K}_{A_i} \boldsymbol{W}_{A_i} = -\boldsymbol{K}_C \boldsymbol{W}_C, \tag{12}$$

where $\boldsymbol{K}_{A_i} = \begin{pmatrix} \boldsymbol{I}_3 & \boldsymbol{0} \\ \boldsymbol{R}_{A_i} & \boldsymbol{I}_3 \end{pmatrix}$, $\boldsymbol{K}_C = \begin{pmatrix} \boldsymbol{I}_3 & \boldsymbol{0} \\ \boldsymbol{R}_c & \boldsymbol{I}_3 \end{pmatrix}$, and $\boldsymbol{R}_{A_i} = \begin{pmatrix} 0 & -z_{A_i} & y_{A_i} \\ z_{A_i} & 0 & -x_{A_i} \\ -y_{A_i} & x_{A_i} & 0 \end{pmatrix}, \boldsymbol{R}_c = \begin{pmatrix} 0 & -z_c & y_c \\ z_c & 0 & -x_c \\ -y_c & x_c & 0 \end{pmatrix}$.

Typically, the foot of the quadruped robot is a simple rubber pad. The contact area between the foot and ground is small. Thus, the moment vector can be neglected, and $\boldsymbol{\tau}_{A_i} = \begin{pmatrix} 0 & 0 & 0 \end{pmatrix}$. Eq. (12) can be modified as

$$\sum_{i=1}^{n} \boldsymbol{K}_{F_i} \boldsymbol{F}_{A_i} = -\boldsymbol{K}_C \boldsymbol{W}_C, \tag{13}$$

where $\boldsymbol{K}_{F_i} = \begin{pmatrix} \boldsymbol{I}_3 \\ \boldsymbol{R}_{A_i} \end{pmatrix}$.

When the position and pose of the robot are known, and the acceleration of the CoM is measured, we can obtain the minimum friction forces to evaluate the stability of the robot, by calculating the least-squares solution of Eq. (13).

In the trotting gait, two standing legs of the quadruped robot in the step forward stage are on the same diagonal of the robot body. Two support points exist on the ground, forming one virtual axis. Therefore, in step forward stage of the trotting gait, the robot body can rotate around this axis and move forward. According to this motion characteristic, when the robot is in the step forward stage with leg 2 and leg 4 in the stance phase, we can simplify the equivalent mechanism of the robot to the mass point model, which is shown in Figure 14(a). Mass point $C$ is connected to axis $A_2A_4$ by two rods. These two rods are connected together through one prismatic joint, and the rod farther away from mass point $C$ is connected to axis $A_2A_4$ through one cylindrical pair in the center of pressure of the two footholds. The premise of this simplified equivalent mechanism is that the robot is in the stable state; in other words, the supporting surface can provide sufficient reaction force to the standing feet. After the switching stage, the robot moves into the next step forward stage. When the robot walks with leg 1 and leg 3 in the stance phase, its simplified equivalent mechanism is as shown as Figure 14(b).

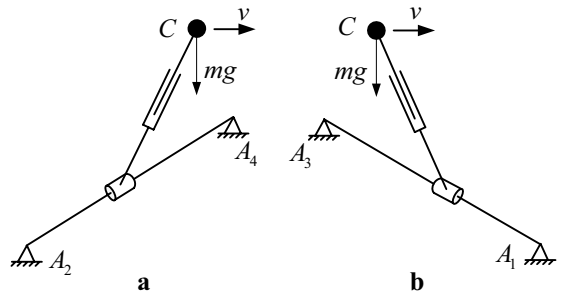


**Figure 14** Simplified mechanism of robot in trotting gait

At any moment during forward stage step of the trotting gait, the ZMP of the quadruped robot must be located on the axis that is determined by the two standing feet if the robot maintains stable. In other words, the resultant force of both gravity and inertia force of mass point crosses with the line established with two stance points. When there is no acceleration component in the vertical direction, we can obtain the minimum acceleration on the horizontal plane, as shown in Figure 15.

According to the geometry in Figure 15, we can obtain

$$ma_{\min} = mg \tan\sigma. \tag{14}$$

The minimum acceleration of mass point $C$ is obtained from following equation:

$$a_{\min} = g \tan\sigma. \tag{15}$$

In this case, the ZMP of the robot is point $D$, which is the center point of the cylindrical joint on axis $A_2A_4$.

In the step forward stage of trotting gait, we can obtain the workspace of the quadruped robot body, using the kinematics model that is established in Section 3. Furthermore, the stability of the robot and the simplified equivalent mechanism are considered. Therefore, we can obtain the stable workspace of the quadruped robot body. When the quadruped robot walks on the ground in trotting gait, its body must be located in the stable workspace. Otherwise, the robot is unstable. The stable workspaces of the equivalent mechanism in the step forward stage of trotting gait is shown in Figure 15, while the friction coefficient equals to 0.05, 0.10, 0.15, and 0.20. As

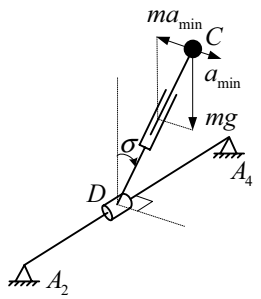


**Figure 15** Force diagram of mass point *C*

shown in Figure 16, a larger friction coefficient results in a larger stable workspace.

## 5 Stride Length of Trotting Gait

The relationship between the stable workspaces of the equivalent mechanisms of two adjacent step forward stages is determined by the robot movement. If there are no any intersections between these workspaces, the robot must walk unstably, or be running or jumping four feet off the ground. Instead, if some intersections exist between the two workspaces, a switching stage will occur in one gait cycle. In the trotting gait of the quadruped robot, switching stages exist. The stable workspaces of the equivalent mechanisms of two adjacent step forward stages must intersect together. Based on this principle, we can obtain the feasible stride length of the trotting gait under certain constraints.

Figure 17 shows the relationship between the stable workspaces of the equivalent mechanisms of two adjacent step forward stages. When the two workspaces' boundary intersection is located exactly on the symmetry axis of the robot body, this condition is assumed as the precondition of the maximum stride length of trotting gait. The maximum stride length can be determined as follows:

$$\lambda = \lambda_1 + \lambda_2, \tag{16}$$

where $\lambda_1$ is the stroke of one step forward stage, and $\lambda_2$ is the stroke of the following step forward stage.

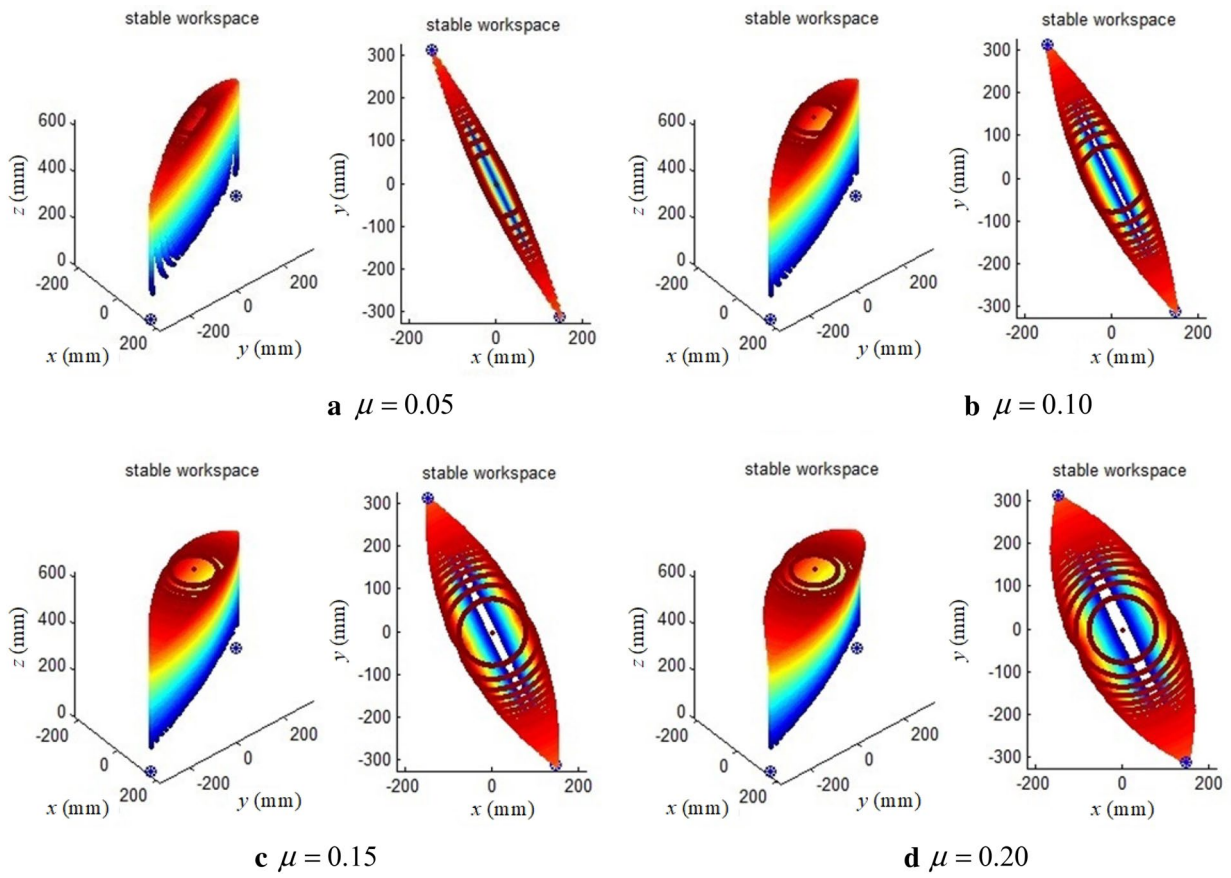


**Figure 16** Stable workspaces of equivalent mechanism under different friction coefficient

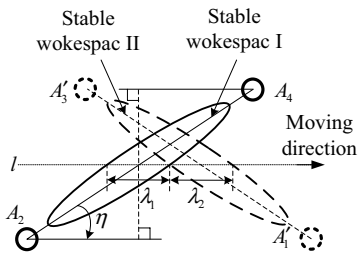


**Figure 17** Two stable workspaces of two adjacent equivalent mechanisms in step forward stages

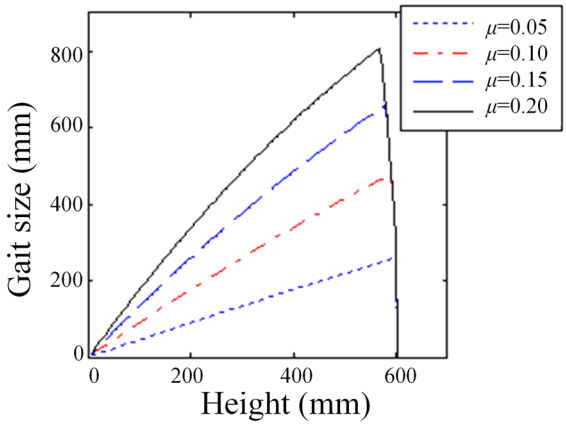


**Figure 18** Maximum stride length under different friction coefficients

Using this method, the maximum stride length can be obtained if the height of the robot body is known. Figure 18 shows the maximum stride length of the trotting gait under different friction coefficients. As shown in the figure, the maximum stride length becomes larger with increasing friction coefficient. On different body heights, the quadruped robot exhibits different maximum stride lengths. When the friction coefficient is known, in the beginning, the stride length becomes larger with increasing body height. At a certain body height, the stride length reaches the largest and subsequently reduces with increasing body height.

## 6 Conclusions

A new method was proposed to analyze the performance of the multilegged robot. With regard to the metamorphic mechanism theory, one gait cycle of the robot was divided into several stages. Each stage of the system consisted of the supporting surface, and the robot exhibited a specific equivalent mechanism. By analyzing this series of equivalent mechanisms, the performance of the multilegged robots was obtained.

A new definition of multilegged robot stability margin was presented to evaluate the robot stability. This definition depended on the friction coefficient between the standing feet and supporting surface. It could be used to estimate whether the robot was in a stable state, regardless of statically stable gait or dynamic stable gait.

The stable workspace of the equivalent mechanism of the robot was defined and simulated based on the kinematics and simplified model of the robot in the step forward stage. Considering the change in body height, the maximum stride length was obtained by analyzing the stable workspaces of the equivalent mechanisms in two adjacent step forward stages of the trotting gait. The simulation results indicated that the stride length increased with the friction coefficient.

**Authors' Contributions**

KX was in charge of the whole analyses and wrote the initial manuscript; PZ assisted with simulation analyses; XD revised the final manuscript. All authors read and approved the final manuscript.

**Authors' Information**

Kun Xu, born in 1981, is currently a lecturer at *Robotics Institute, Beihang University, China*. He received his PhD degree from *Beihang University, China*, in 2012. His research interests include legged robot and Space deployable structure.

Peijin Zi, born in 1993, is currently a PhD candidate at *Robotics Institute, Beihang University, China*.

Xilun Ding, born in 1967, is currently a professor and a PhD candidate supervisor at *Robotics Institute, Beihang University, China*. He received his PhD degree from *Harbin Institute of Technology, China*, in 1997. His research interests include the dynamics of compliant mechanical systems and robots, nonholonomic control of space robots, dynamics and control of aerial robots, and biomimetic robots.

**Competing Interests**

The authors declare that they have no competing interests.

**Funding**

Supported by National Natural Science Foundation of China (Grant Nos. 51775011, 91748201).

## Publisher's Note



Received: 9 August 2017 Accepted: 10 January 2019
Published online: 03 February 2019

**References**

[1] S Hirose. Three basic types of locomotion in mobile robots. *5th International Conference on Advanced Robotics 'Robots in Unstructured Environments'*, Pisa, Italy, June 19–22, 1991. New York: IEEE, 1991: 12–17.

[2] J S Dai, J R Jones. Mobility in metamorphic mechanisms of foldable/erectable kinds. *ASME Transaction, Journal of Mechanical Design*, 1999, 121(3): 375–382.

[3] J S Dai, Q X Zhang. Metamorphic mechanism and their configuration models. *Chinese Journal of Mechanical Engineering*, 2000, 13(3): 212–218.

[4] K Xu, X Ding. Typical gait analysis of a six-legged robot in the context of metamorphic mechanism theory. *Chinese Journal of Mechanical Engineering*, 2013, 26(4): 771–783.

[5] W K Zhen, K Xi, X S Zhang, et al. Gait planning of a novel metamorphic quadruped robot. *Journal of Mechanical Engineering*, 2016, 52(11): 26–33. (in Chinese)

[6] S Hirose. A study of design and control of a quadruped-walking vehicle. *Robotics Research*, 1984, 3(2): 113–133.

[7] J R Rebula, P D Neiiliaus, B V Bonnlander, et al. A controller for the LittleDog quadruped walking on rough terrain. *IEEE International Conference on Robotics and Automation*, Roma, Italy, April 10–14, 2007. New York: IEEE, 2007: 1467–1473.

[8] G Nelson, K Blankespoor, M Raibert. Walking BigDog: insights and challenges from legged robotics. *Journal of Biomechanics*, 2006, 39(6): S360–S360.

[9] R Sparrow. Kicking a robot dog. *ACM/IEEE International Conference on Human-Robot Interaction*, Christchurch, New Zealand, March 7–10, 2016. New York: IEEE, 2016: 229–229.

[10] C Semini, N G Tsagarakis, E Guglielmino. Design of HyQ-a hydraulically and electrically actuated quadruped robot. *Proceedings of the Institution of Mechanical Engineers, Part I: Journal of Systems and Control Engineering*, 2011, 225(6): 831–849.

[11] T Boaventura, J Buchli, C Semini, et al. Model-based hydraulic impedance control for dynamic robots. *IEEE Transactions on Robotics*, 2015, 31(6): 1324–1336.

[12] C Semini, V Barasuol, T Boaventura, et al. Towards versatile legged robots through active impedance control. *International Journal of Robotics Research*, 2015, 34(7): 1003–1020.

[13] J H Dong, O S Sang, J Lee, et al. High speed trot-running: Implementation of a hierarchical controller using proprioceptive impedance control on the MIT Cheetah. *International Journal of Robotics Research*, 2014, 33(11): 1417–1445.

[14] S Seok, A, Wang Y C Meng, et al. Design principles for energy-efficient legged locomotion and implementation on the MIT cheetah robot. *IEEE/ASME Transactions on Mechatronics*, 2015, 20(3): 1117–1129.

[15] H W Park, S Park, S Kim. Variable-speed quadrupedal bounding using impulse planning: Untethered high-speed 3D Running of MIT Cheetah 2. *IEEE International Conference on Robotics and Automation*, May 26–30, 2015 Washington, USA. New York: IEEE, 2015: 5163–5170.

[16] D J Hyun, J Lee, S Park, et al. Implementation of trot-to-gallop transition and subsequent gallop on the MIT Cheetah I. *International Journal of Robotics Research*, 2016, 35(13): 1627–1650.

[17] P M Wensing, A Wang, S Seok, et al. Proprioceptive actuator design in the MIT Cheetah: Impact mitigation and high-bandwidth physical interaction for dynamic legged robots. *IEEE Transactions on Robotics*, 2017, 33(3): 509–522.

[18] H W Park, P M Wensing, S Kim. High-speed bounding with the MIT Cheetah 2: Control design and experiments. *International Journal of Robotics Research*, 2017, 36(2): 167–192.

[19] S Kitano, S Hirose, G Endo, et al. Development of lightweight sprawling-type quadruped robot TITAN-XIII and its dynamic walking. *IEEE/RSJ International Conference on Intelligent Robots and Systems*, Tokyo, Japan, November 3–7, 2013. New York: IEEE, 2013: 6025–6030.

[20] S Kitano, S Hirose, A Horigome, et al. TITAN-XIII: sprawling-type quadruped robot with ability of fast and energy-efficient walking. *Robomech Journal*, 2016, 3(8): 1–16.

[21] C Gehring, S Coros, M Hutter, et al. Control of dynamic gaits for a quadrupedal robot. *IEEE International Conference on Robotics and Automation*, Karlsruhe, Germany, May 6–10, 2013. New York: IEEE, 2013: 3287–3292.

[22] M Hutter, H Sommer, C Gehring, et al. Quadrupedal locomotion using hierarchical operational space control. *International Journal of Robotics Research*, 2014, 33(8): 1047–1062.

[23] M Hutter, C Gehring, D Jud, et al. ANYmal - a highly mobile and dynamic quadrupedal robot. *IEEE/RSJ International Conference on Intelligent Robots and Systems*. Daejeon, Korea, October 8–9, 2016. New York: IEEE, 2016: 38–44.

[24] M Hutter, C Gehring, A Lauber, et al. ANYmal - toward legged robots for harsh environments. *Advanced Robotics*, 2017, 31(17): 1–14.

[25] M Hutter, R Diethelm, S Bachmann, et al. Towards a generic solution for inspection of industrial sites *Field and Service Robotics*. Berlin: Springer International Publishing, 2018

[26] M Neunert, M Stäuble, M Giftthaler, et al. Whole-body nonlinear model predictive control through contacts for quadrupeds. *IEEE Robotics & Automation Letters*, 2018, 3(3): 1458–1465.

[27] B Li, Y B Li, X W Rong, et al. Trotting gait planning and implementation for a little quadruped robot. *Electronics and Signal Processing*, 2011, 97: 195–202.

[28] X W Rong, Y B Li, J Ruan, et al. Design and simulation for a hydraulic actuated quadruped robot. *Journal of Mechanical Science & Technology*, 2012, 26(4): 1171–1177.

[29] C Hui, M Jian, X W Rong, et al. Design and implementation of SCalf, an advanced hydraulic quadruped robot. *Robot*, 2014, 36(4): 1–7. (in Chinese)

[30] G T Zhang, Z Y Jiang, Y B Li, et al. Active compliance control of the hydraulic actuated leg prototype. *Assembly Automation*, 2017, 37(6): 356–368.

[31] X Tian, F Gao, X B Chen. Mechanism design and comparison for quadruped robot with parallel-serial leg. *Journal of Mechanical Engineering*, 2013, 49(6): 81–88. (in Chinese)

[32] X B Chen, F Gao, C K Qi, et al. Spring parameters design to increase the loading capability of a hydraulic quadruped robot. *IEEE International Conference on Advanced Mechatronic Systems*, Luoyang, China, September 25–27, 2013. New Yok: IEEE, 2013: 535–540.

[33] J Q Zhang, F Gao, X L Han, et al. Trot gait design and CPG method for a quadruped robot. *Journal of Bionic Engineering*, 2014, 11(1): 18–25.

[34] F Gao, C K Qi, Q Sun, et al. A quadruped robot with parallel mechanism legs. *IEEE International Conference on Robotics and Automation (ICRA)*, Hong Kong, China, June 1–5, 2014: 2566–2566.

[35] X B Chen, F Gao, C K Qi, et al. Spring parameters design for the new hydraulic actuated quadruped robot. *Journal of Mechanisms & Robotics*, 2014, 6(2): 97–110.

[36] X B Chen, F Gao, C K Qi, et al. Gait planning for a quadruped robot with one faulty actuator. *Chinese Journal of Mechanical Engineering*, 2015, 28(1): 11–19.

[37] X Tian, F Gao, C Qi, et al. External disturbance identification of a quadruped robot with parallel–serial leg structure. *International Journal of Mechanics & Materials in Design*, 2016, 12(1): 109–120.

[38] X B Chen, F Gao. Energy expenditure of trotting gait under different gait parameters. *Chinese Journal of Mechanical Engineering*, 2017, 30(4): 1–8.

[39] M J Song, C J Ding, C J Yu. Workspace analyzing for hybrid serial-parallel mechanism of a new bionic quadruped robot. *Applied Mechanics & Materials*, 2015, 713–715: 837–840.

[40] K Xu , X Ding. Gait analysis of a radial symmetrical hexpod robot based on parallel mechanisms. *Chinese Journal of Mechanical Engineering*, 2014, 27(5): 867–879.

[41] D Zhao, X Jing, W Dan, et al. Gait Definition and successive gait-transition method based on energy consumption for a quadruped. *Chinese Journal of Mechanical Engineering*, 2012, 25(1): 29–37.

[42] Y Fukuoka, H Kimura. Dynamic locomotion of a biomorphic quadruped 'Tekken' robot using various gaits: walk, trot, free-gait and bound. *Applied Bionics & Biomechanics*, 2009, 6(1): 63–71.

[43] M H Raibert. Trotting, pacing and bounding by a quadruped robot. *Journal of Biomechanics*, 1990, 23(1): 79–98.

[44] E Garcia, J Estremera, PGD Santos. A comparative study of the stability margins for walking machines. *Robotcis*, 2002, 20(6): 595-606.

[45] M Vukobratovic. On the stability of anthropomorphic systems. *Mathematical Biosciences*, 1972, 15(1): 1–37.